science, engineering and health studies

Research Article

Science, Engineering and Health Studies
https://lio1.tci-thaijo.org/index.php/sehs
ISSN (Online): 2630-0087

The effect of mineralogy and microfabric on the shear strength of clayey from the Trusmardi formation in Bundu Tuhan, Sabah

Nur Ayu Sufiah Khairul[1], *Hennie Fitria W. S. Erfen*[1,2], *and Baba Musta*[1,2*]

[1] Faculty of Science and Technology (FST), Universiti Malaysia Sabah, Kota Kinabalu, Sabah 88400, Malaysia
[2] Natural Disaster Research Centre (NDRC), Faculty of Science and Technology, Universiti Malaysia Sabah, Kota Kinabalu, Sabah 88400, Malaysia

***Corresponding author**:
Baba Musta
babamus@ums.edu.my

***Received**: 3 April 2024*
***Revised**: 7 October 2024*
***Accepted**: 15 October 2024*
***Published**: 31 December 2025*

***Citation**:
Khairul, N. A. S., Erfen, H. F. W. S., & Musta, B. (2025). The effect of mineralogy and microfabric on the shear strength of clayey from the Trusmardi formation in Bundu Tuhan, Sabah. Science, Engineering and Health Studies, 19, 25020010.

ABSTRACT

Soil instability, including slope failure and creeping, frequently occurs in the research area of Bundu Tuhan, Sabah. The lithology in this region primarily comprises interbedded sandstone, metasandstone, shale, and argillite from the Trusmadi formation. Intense weathering contributes to the formation of thick, clayey soil profiles. Geotechnical laboratory tests classified clayey soils from three distinct locations as poorly sorted materials of sandy-silty clay and silty clay textures. X-ray diffractograms revealed the presence of kaolinite and illite in the clayey soils. Electron microscopy images demonstrated the microfabric characteristics of clayey soil, such as pseudohexagonal plate shapes of kaolinite and ribbon-like projections of illite. Shear strength analysis results of the clayey soil samples indicated values ranging from 128.28 to 155.01 kPa, classifying the soils as strong. The presence of clay minerals in the soil facilitated water adsorption into the mineral structure, potentially softening the soil and reducing its shear strength. Understanding the mineralogical composition of these soils is essential for mitigating soil instability by implementing measures like lime treatment on slopes, particularly in high-risk areas.

Keywords: soil movement; clayey soil; microfabric; mineralogy; shear strength

1. INTRODUCTION

The occurrence of mass movement and slope failure in the research area has been extensively examined by earlier studies (Roslee et al., 2005; Jr. Joe et al., 2018). The significance of weak soil planes on the sliding surface cannot be overstated as a leading contributor to slope failures (Roslee, 2020). The soil composition in the area predominantly stems from the weathered rock of the Trusmadi formation. Consisting of interbedded sandstone, metasandstone, shale, and argillite ranging from the Paleocene to the Middle Eocene period, the Trusmadi formation has been well-documented (Jacobson, 1970). The presence of well-graded and poorly sorted clayey materials resulting from weathering processes influences apparent soil cohesion due to the existence of clay minerals. Landslides are triggered by a disruption in the equilibrium between stress and strength of the slope materials, ensuing when shear stress or applied loads exceed the shear strength or maximum resistance of the material (Yalcin, 2007). Accordingly, this research delves into the behavior of clay particles concerning the shear strength of the entire sample. These clay minerals, however, can impede the slope materials' stability due to external factors like heavy rainfall, where data from the Malaysian Meteorological Department (Sabah) for the

years 2012 to 2020 reveals precipitation levels exceeding 4000 mm annually, categorizing the area as very wet (Smith et al., 2006; Azizi et al., 2020). The clay minerals' ability to expand and contract based on moisture conditions results in reduced soil cohesion when cracks develop.

The study area in Bundu Tuhan, encompassing about 100 km^2, is situated on the West Coast of Sabah, delineated between Kota Belud and Kundasang, with coordinates ranging from 116°028'11'' to 116°033'38'' East longitude and 5°057'23'' to 6°002'52'' North latitude. Geologically, the dominant formations in the research area are the Trusmadi formation, dating from the Paleocene to the Middle Eocene, and the Crocker formation, from the Late Eocene to Early Miocene. These formations are demarcated by a significant North-South-oriented wrench fault with dextral displacement, as depicted in Figure 1. Additionally, minor exposure of igneous rocks is observed, comprising the Triassic to Cretaceous crystalline basement and the Late Miocene to Pliocene igneous intrusion (Jr. Joe et al., 2018; Sanudin & Baba, 2007). Sampling sites were strategically selected based on observable signs of slope instability and the high vulnerability of infrastructure and local residents in the area, such as undulating surfaces, road surface cracks, erosion, and leaning structures, as illustrated in Figure 2.

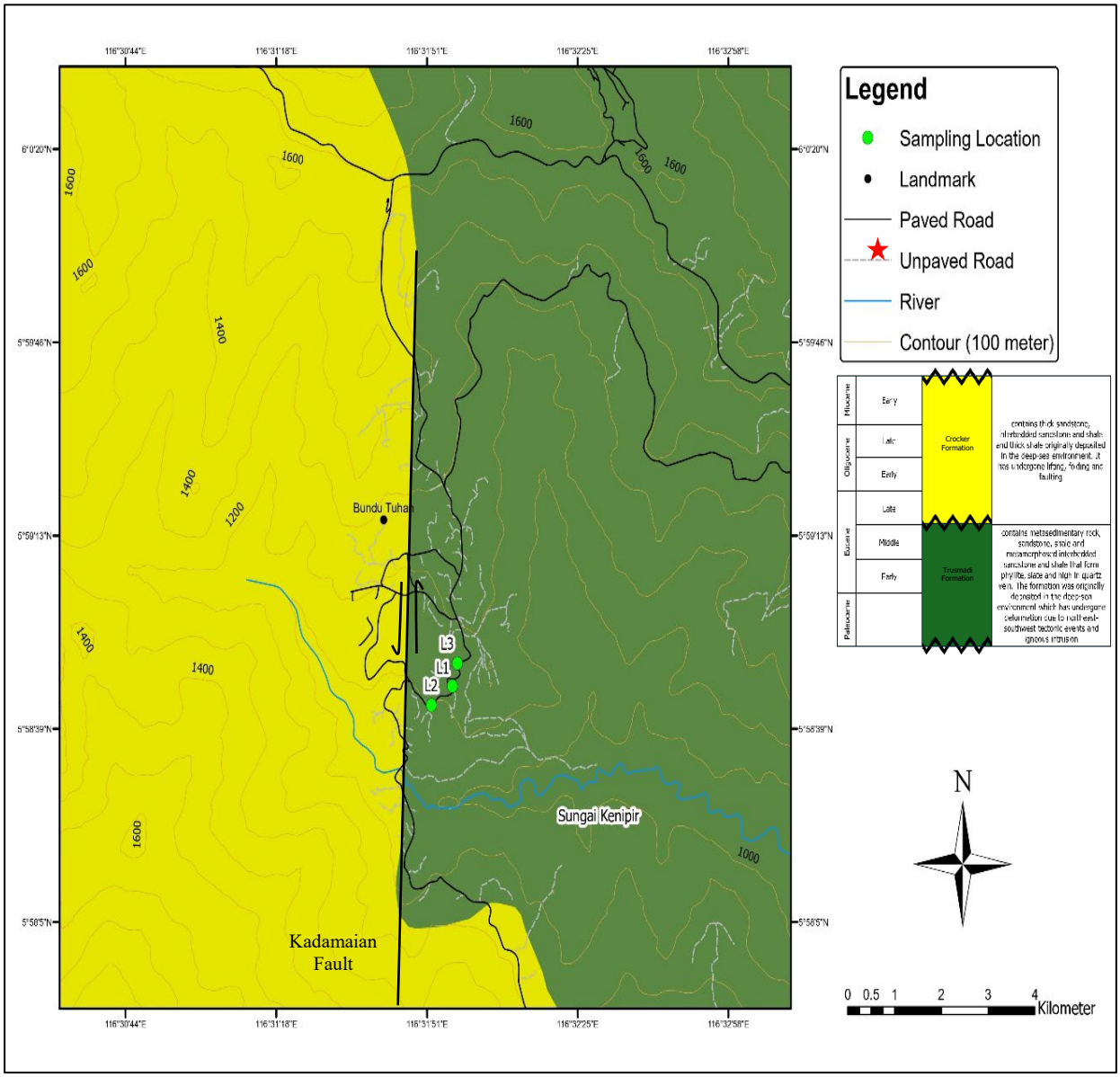

Figure 1. Geological map of the study area

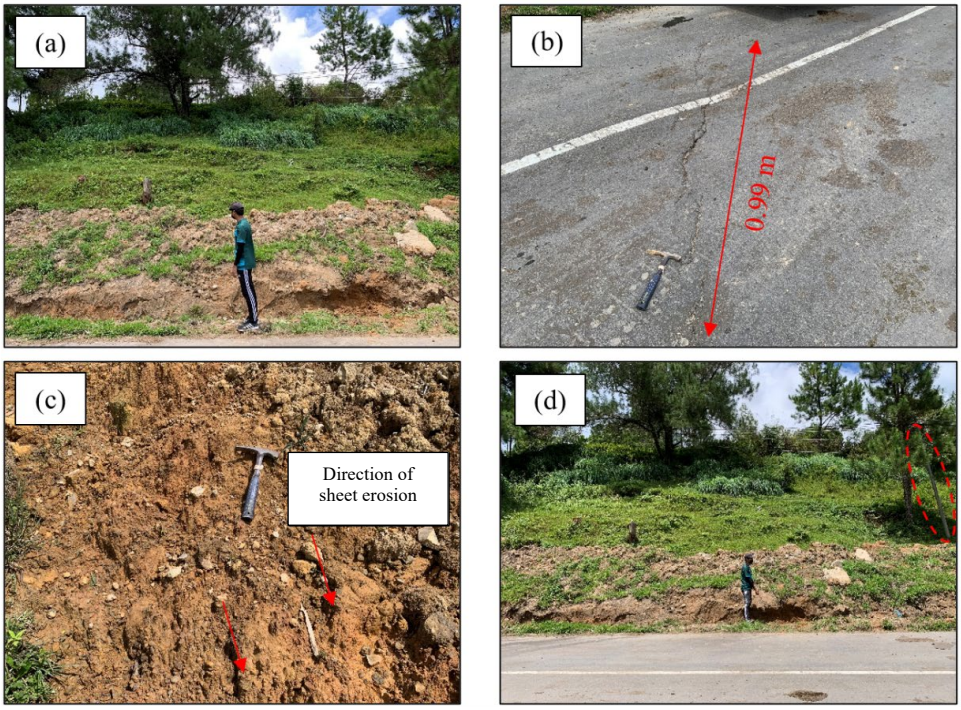

Figure 2. Signs of slope instability were found in the study area; (a) an undulating surface on the slope surface (height of surveyor: 1.70 m), (b) a longitudinal on the road surface, (c) severe sheet erosion on the slope surface, and (d) a tilting pole at the toe of the failing slope

2. MATERIALS AND METHODS

Geotechnical and mineralogical analyses are essential to assess mineralogy's impact on clayey soil's shear strength. Both disturbed and undisturbed samples were gathered from three specified sections of the Trusmadi formation's slopes – L1, L2, and L3 (Figure 3). The disturbed samples were stored in plastic bags, whereas the undisturbed samples were obtained using PVC tubes and carefully coated with paraffin wax to maintain their original moisture content.

2.1 Geotechnical analysis

Basic soil properties and geotechnical analyses were carried out to determine the strength of clayey soil at three sampling sites. The analyses included testing for moisture content, particle size distribution, soil specific gravity, Atterberg limits, Proctor compaction test, triaxial compression test, and permeability test (falling head). These assessments were conducted in accordance with the protocols outlined in the American Society for Testing and Materials Code of Practice ASTM D698-2012 and the British Standard Code of Practice BS 1377-1990 (Methods of Test for Soils for Civil Engineering Purpose) (ASTM International, 2012; British Standards Institution, 1990).

The moisture content of soil was determined according to BS 1377-Part 2: 3.2, using an oven-dry method at 105°C. Particle size distribution was analyzed using two methods: the pipette method (BS 1377-Part 2: 9.4) for silt and clay percentages determination post-deposition, and the dry sieve method (BS 1377-Part 2: 9.3) for the sand percentage based on retained grains post-sieving. The soil-specific gravity, as per BS 1377-Part 2: 8.3, was determined using the pycnometer method that involves creating a vacuum and immersing the apparatus in a water bath to calculate the ratio of soil density to water density.

The plasticity chart was used to determine the Atterberg limits, which include the plastic limit (BS 1377-Part 2: 5), liquid limit (BS 1377-Part 2: 4.3 & 4.4), and plasticity index (BS 1377-Part 2: 5). These tests are crucial for clayey soils to evaluate their plasticity degree (Terzaghi & Peck, 1996).

The dynamic compaction method was utilized on a soil sample that received 27 blows from a standard hammer as per the Proctor compaction test (BS 1377-Part 4). This test yields the maximum dry density (MDD) and optimum moisture content (OMC) values to ascertain the necessary compaction for achieving maximum strength and compressibility of the soil sample in the research location. The MDD and OMC values are crucial for determining the precise quantities of soil sample and water required for preparation in the triaxial compression and permeability tests.

Using a semi-automatic compression machine, the triaxial compression test (BS 1377-Part 8) applies the static compaction method to an undisturbed soil sample. This method is utilized to determine and classify shear strength properties through the consolidated undrained test following the classification system (Terzaghi & Peck, 1996). Moreover, the permeability of fine-grain samples can be assessed and categorized through the permeability test (BS 1377-Part 5), which typically runs for a duration of six h (Terzaghi & Peck, 1996).

2.2 Mineralogy analysis

Mineralogical analysis is crucial for recognizing a soil sample's mineral composition and microstructure, which significantly affects its shear strength properties. One of

the common methods used for this purpose is X-ray diffraction (XRD), which is employed to identify the primary minerals present in a finely crushed soil sample (Andrei et al., 2015). Subsequently, the identification of clay minerals revealed in the XRD analysis was further confirmed through scanning electron microscopy (SEM) analysis, which helps to identify their distinct patterns. These analyses were conducted in accordance with the guidelines provided in the British Standard Code of Practice BS EN 13925-2003 and BS 1SO 16700-2016, respectively (British Standards Institution, 2003, 2016).

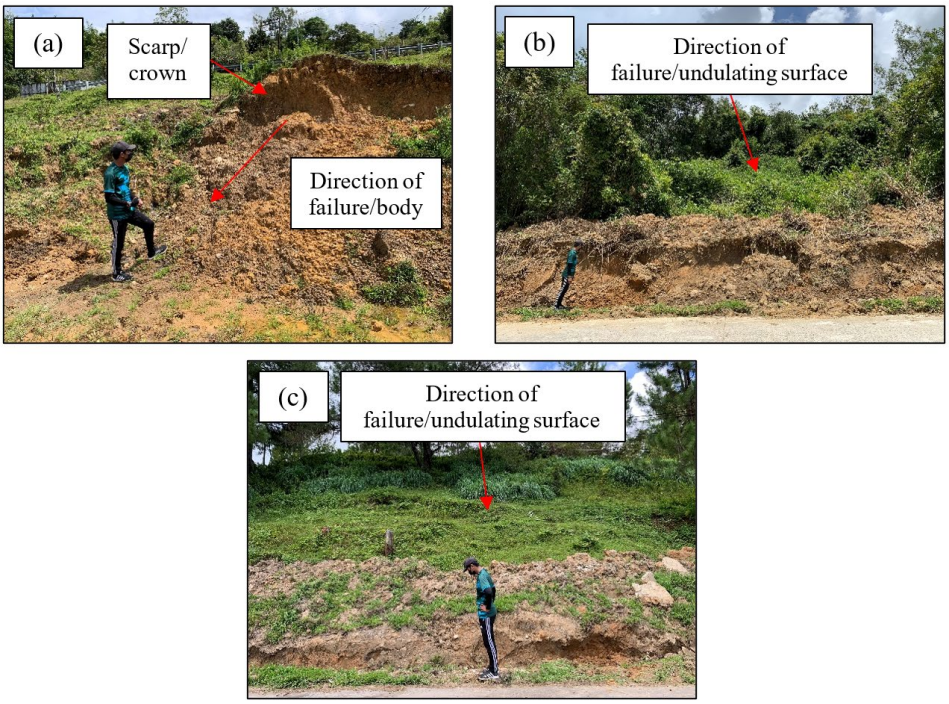

Figure 3. Failing slopes of Trusmadi formation in the study area; (a) rotational debris slide on the slope from location L1, (b) soil creeping on the slope from location L2, and (c) soil creeping on the slope from location L3

3. RESULTS AND DISCUSSION

3.1 Basic properties

Table 1 presents a detailed analysis of clayey soils obtained from three sites (L1, L2, and L3). The slopes at these sites exhibited high weathering, with residual soil being predominant, categorized as grade VI. Soil from L1 is identified as sandy-silty clay, whereas L2 and L3 as silty clay (Head, 1982). The specific gravity readings fall below the standard range of 2.70 to 2.80, resulting in reduced soil density (Bowles, 2012). The soil samples are classified as high-plasticity material based on their liquid limit and plasticity index percentages (Terzaghi & Peck, 1996). For optimal performance, the soil samples should be compacted within the specified range from 25.0% to 26.4% for moisture content and 1.45 to 1.54 mg/m^3 for maximum dry density, ensuring their maximum bearing capacity (Balasubramanian, 2017). As per the triaxial compression test results, the soil samples exhibit strength, while the permeability rate across all samples is deemed impermeable (Terzaghi & Peck, 1996).

3.2 Engineering properties

Figure 4 illustrates the stress-strain curve, depicting the correlation between axial stress during compression and axial strain as indicated by the specimen's height. Three intact soil specimens are extracted from each soil sample and subjected to compression under varying cell pressure conditions: 25 kPa (blue line), 50 kPa (orange line), and 75 kPa (grey line). The stress-strain curves of the soil samples from the distinct locations display a ductile failure mode, initially demonstrating a direct relationship between stress and strain, transitioning to an inverse proportionality post reaching the peak axial stress.

Ductile materials exhibit high ductility, allowing them to endure substantial strains before fracturing, a characteristic commonly found in highly plastic materials like wet clay (Roylance, 2001). For instance, the mineral illite in clay plays a crucial role in enhancing plasticity by absorbing more water into its mineral structure compared to kaolinite. The higher the ductility of a material, the more pronounced the curve will be. In this context, the soil samples from location L1 display the most pronounced curve compared to those from locations L2 and L3, indicating superior ductile capacity as supported by the highest value of unconfined compressive strength (qu). This indicates the ability of the material to endure significant deformations without failing. On the other hand, samples from location L2 exhibit an intermediate behavior with a less steep curve than those from location L1 but still showing notable ductility and qu values. Conversely, samples from location L3 present the least steep curve among the three locations, signifying lower ductility and qu values, suggesting a tendency to deform less before failing and a reduced resistance to compression strains (Mashiri et al., 2015).

Table 1. Geotechnical properties of the clayey soil samples from Trusmadi formation

Slope name	L1	L2	L3	Classification
Weathering grade	VI	VI	VI	Residual soil (Head, 1982)
Moisture content (%)	25.98	37.10	34.98	Wet to very wet (Malaysian Meteorological Department (Sabah), 2022)
Sand (%)	11.20	11.20	10.51	L1 is classified as silty clay with sand, while L2 and
Silt (%)	64.22	51.89	56.19	L3 are classified as silty clay (Head, 1982)
Clay (%)	24.57	36.91	33.30	
Specific gravity	2.61	2.61	2.64	Inorganic clay (Bowles, 2012)
Plastic limit (%)	31.72	31.47	34.52	-
Liquid limit (%)	55.64	53.15	53.37	-
Plasticity index (%)	23.91	21.68	18.86	High plasticity material (Terzaghi & Peck, 1996)
Optimum moisture content, OMC (%)	25.10	25.00	26.40	The soil in the area should be compacted at calculated OMC and MDD for maximum strength
Maximum dry density, MDD (Mg/m^3)	1.54	1.53	1.45	(Balasubramanian, 2017)
Shear strength, Ƭ (kPa)	155.01	143.82	128.28	Strong soil (Terzaghi & Peck, 1996)
Permeability (m/s)	6.671×10^{-9}	5.271×10^{-9}	8.515×10^{-9}	Impermeable soil (Terzaghi & Peck, 1996)

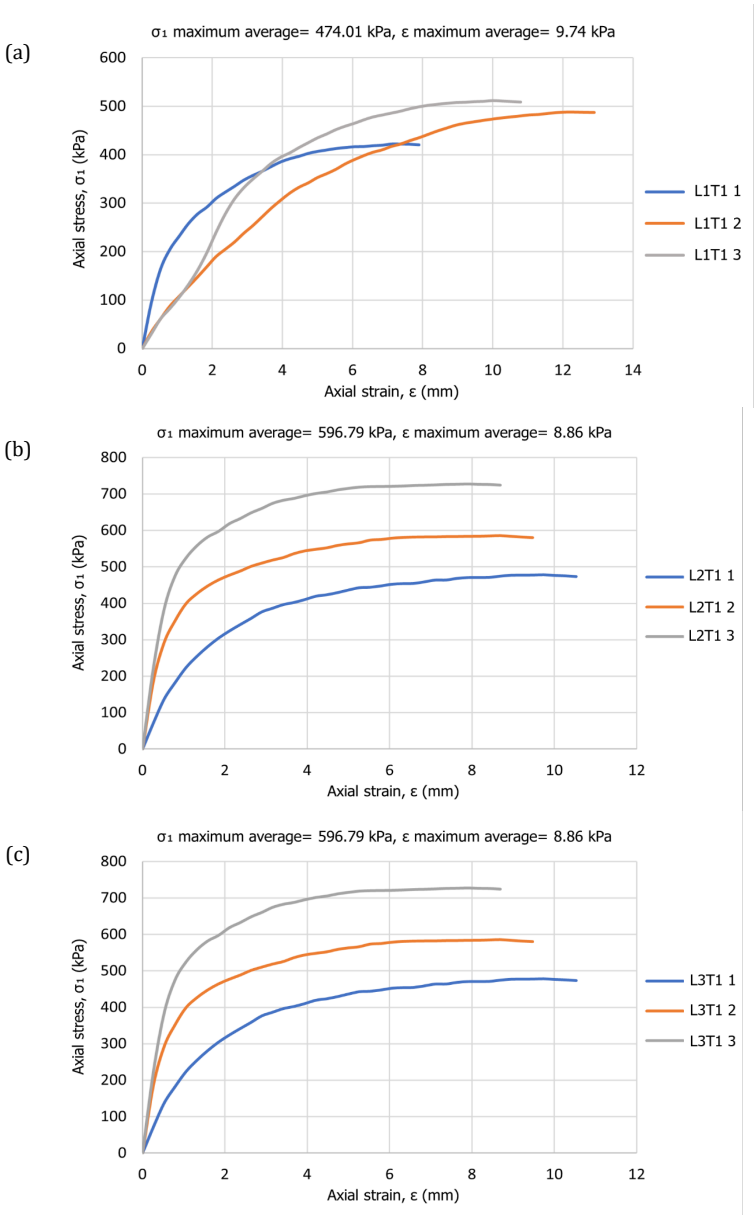

Figure 4. Stress-strain curve of the clayey soil samples from Trusmadi formation; (a) location L1, (b) from location L2, and (c) from location L3

Figure 5 illustrates the Mohr-Coulomb criterion, depicting the relationship between shear stress and normal stress. Shear stress is determined by the cohesion and friction angles, with cohesion being dominant, especially in fine-grained soil (Terezie et al., 2016). Soil samples from location L1 exhibit the largest Mohr-Coulomb circle radius compared to locations L2 and L3, indicating higher shear strength supported by significant cohesion and friction angles, resulting in increased resistance to shear forces.

Moreover, soil samples from L2 show an intermediate-sized Mohr-Coulomb circle, reflecting substantial shear strength but lower than that of L1, suggesting a moderately effective combination of cohesion and friction angles in providing shear resistance. On the other hand, soil samples from L3 display the smallest Mohr-Coulomb circle radius, pointing to the lowest shear strength among the three locations. These samples exhibit lower cohesion and friction angles, leading to reduced ability to withstand shear stress.

3.3 Mineralogy and microfabric

Figure 6 displays the XRD results for the soil samples. The XRD illustrates the relationship between intensity, indicating well-formed crystals, denoted by higher peaks, and 2θ, confirming the existing mineral type with at least three prominent peaks. The XRD of the clayey soils indicated the presence of silicate mineral quartz alongside clay minerals kaolinite and illite. Concerning the abundance of clay minerals, the majority of samples reveal that kaolinite's peak prominence surpasses that of illite, except for L1S3 and L2S3, with the highest average intensity value for illite.

Each specimen's XRD is complemented by its microscopy image from SEM analysis, showcasing the microfabric of clayey soil, depicting interactions between small clay platelet groups, assemblages of clay particles, and the presence of pore spaces within clay particles. Figure 7 exhibits the SEM images of clayey soils from three distinct locations, represented by solid-form images. Clayey soil nature is commonly characterized by an increased proportion of clay minerals. The clay mineral framework comprises two unit layers, tetrahedral and octahedral, that bind together to form an aluminosilicate layer (Juergen, 2011). Consequently, well-crystallized authigenic kaolinite denoted by K is present in all soil samples. This clay mineral manifests pseudohexagonal plate shapes stacked face to face, with crystal diameters ranging from two to five μm. The proximity of kaolinite crystals is due to strong hydrogen bonds among aluminosilicate layers. Additionally, fine-grained authigenic illite denoted by I is evident in all soil samples, presenting thin flakes with ribbon-like projections. The distribution of illite crystals is more dispersed due to weaker ionic bonds of potassium ions within aluminosilicate layers. Alongside clay minerals, silicate minerals such as quartz overgrowths are also visible in the electron microscopy images of the soil samples from location L3, denoted by Q. These minerals display symmetry properties of a helix on the atomic lattice and form individual crystals without layering (Welton, 1984). Moreover, the porosity percentage in the specimens can be approximated from the electron microscopy images, typically falling between 51% and 58%.

3.4 Effect of the clay mineral on shear strength

Clay minerals are formed as a byproduct of the chemical weathering processes commonly occurring in sedimentary rock. Consequently, clay minerals constitute the predominant mineral composition in clayey soils (Nelson, 2014). The shear strength of soil masses denotes the internal resistance per unit area that the soil can exert to prevent failure and sliding along any internal plane within the soil body (Jackson & Dhir, 1996). In the examined area, the undisturbed, saturated, and consolidated soil samples exhibited shear strength values ranging from 128.28 kPa to 155.01 kPa, categorizing the soil as strong. However, disturbed soil samples lacking such reinforcement measures inherently display lower shear strength, rendering them highly vulnerable to landslides. This susceptibility is attributed to the abundance of clay minerals like kaolinite and illite, which play a significant role in these occurrences. The clay mineral structure comprises a tetrahedral and octahedral units that are bonded together, forming an aluminosilicate layer. This structure triggers several key factors leading to a reduction in shear strength (Juergen, 2011).

The primary concern in geotechnical studies often revolves around the swell-shrink behavior of clay minerals in response to varying moisture levels (Birchmier, 2005). Through mineralogical analysis, the prevalent clay minerals identified in the study region were kaolinite and illite. Kaolinite is classified as a non-swelling clay mineral characterized by a one unit layer of tetrahedral and one unit layer of octahedral structure bonded together by strong hydrogen bonds (Juergen, 2011). Hydrogen bonds result in a lower cation exchange capacity, leading to minimal fluctuations in expansion and shrinkage rates as only a limited amount of water molecules can penetrate its structure. On the other hand, illite is a swelling clay mineral formed by two unit layers of tetrahedral and one unit layer of octahedral structure bound by potassium ions, creating spaces that facilitate higher cation exchange capacity, enabling greater water absorption compared to kaolinite (Valášková & Martynková, 2012).

Previous research has indicated that cracks may develop during the swell-shrink cycles of clay minerals, often causing infrastructure failures built on clayey soils (Zhou et al., 2021). These cracks result from two mechanisms: a) shrinkage-cracking and b) swelling-cracking (Zhou et al., 2021). Shrinkage-cracking occurs when clay minerals lose moisture in dry conditions, inducing tensile stress on the mineral's surface due to differential evaporation rates inside and outside the mineral. The development of tensile cracks is initiated when the stress surpasses the tensile strength of the mineral. Conversely, swelling-cracking occurs when clay minerals absorb moisture in humid conditions. Non-uniform moisture absorption due to variations in clay mineral properties prompts internal swelling stress, softening the soil and breaking the bonds between clay particles, leading to swelling cracks (Zhou et al., 2021; Soehady Erfen et al., 2018). These cracks weaken the interparticle bonds in the clayey soil, thereby reducing its shear strength, as observed at locations L1, L2, and L3 in the study area.

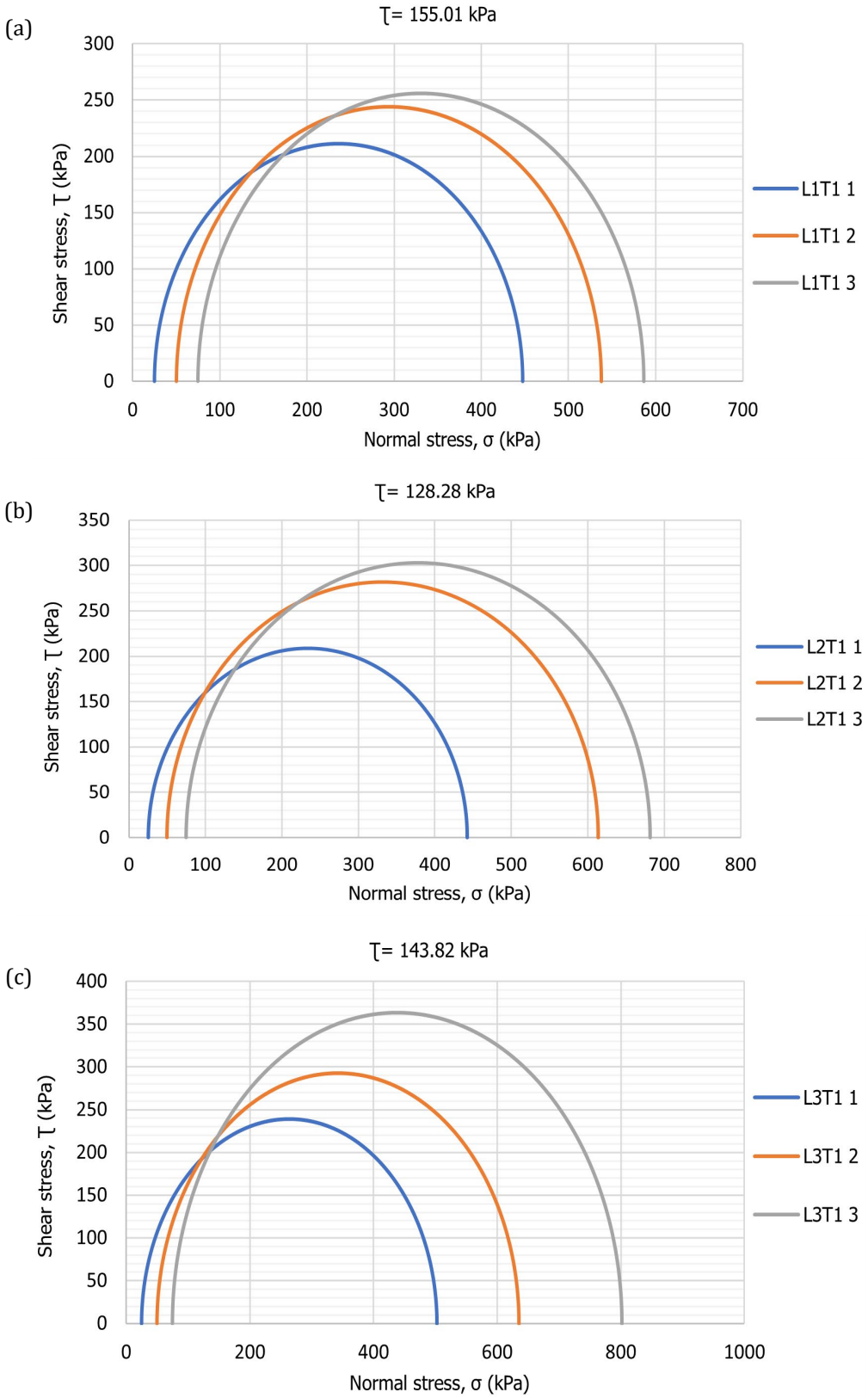

Figure 5. Mohr coulomb circle of the clayey soil samples from Trusmadi formation; (a) location L1, (b) location L2, and (c) location L3

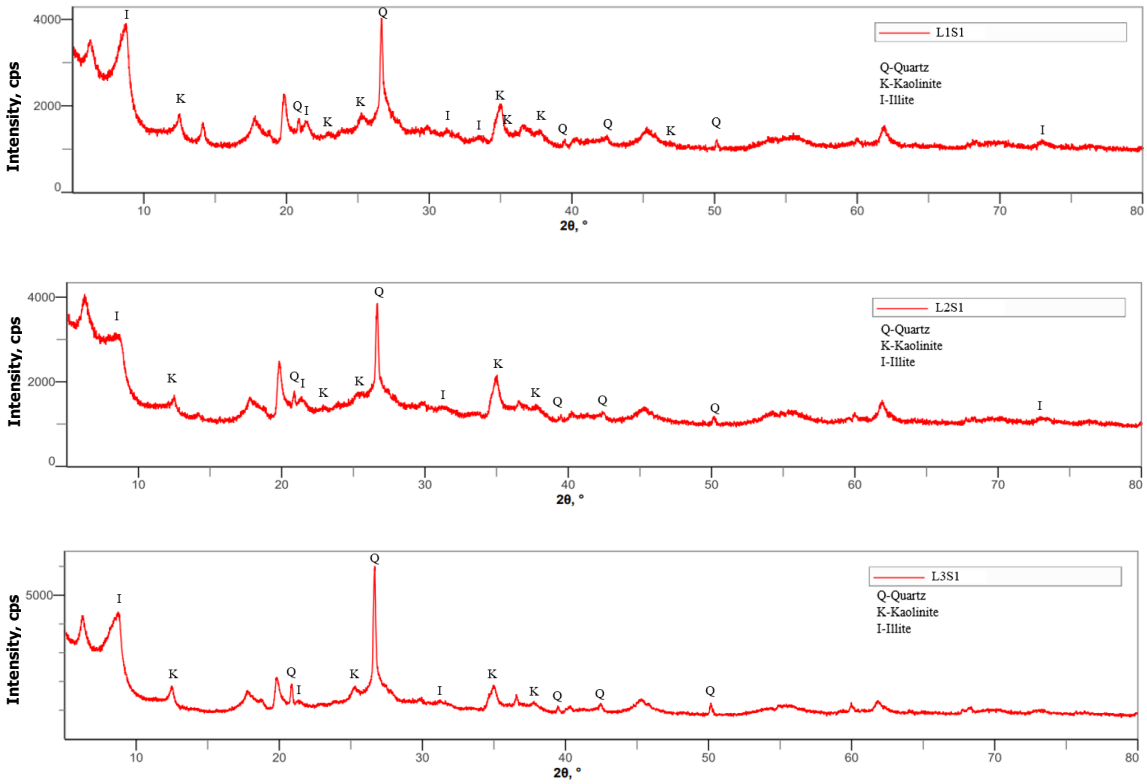

Figure 6. X-ray diffractograms of the clayey soil samples from the Trusmadi formation

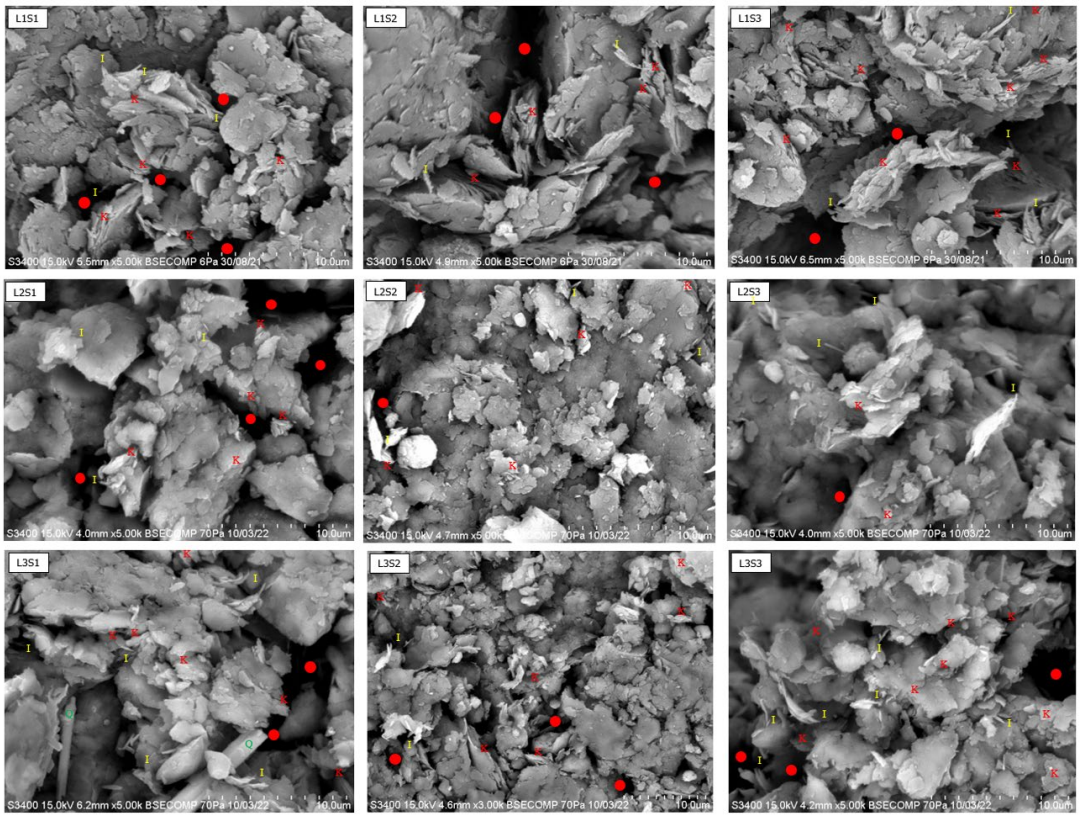

Figure 7. Electron microscopic images of the clayey soil samples from the Trusmadi formation
Note: kaolinite (K), illite (I), and quartz (Q)

Clayey soils with a high clay mineral content rely on cohesion forces for shear strength, requiring water molecules to initiate this force (Bullock et al., 1988). The second factor influencing these soils is heavy rainfall, indirectly impacting them by increasing the water content. In the study area, soil moisture content ranges from 25.98% to 37.10%, classified as wet to very wet due to the region's high average annual rainfall, leading to increased water infiltration. As water fills the voids between clay particles, displacing air molecules, the soil becomes fully saturated, resulting in positive pore water pressure (Suhaimi & Selaman, 2013). Pore water pressure, caused by water molecules in pore spaces, can reduce cohesion forces and shear strength when pressures are elevated (Prasad, 2017).

The third factor concerns the porosity and permeability of the clay particles. Porosity estimates the void spaces in the soil mass, while permeability measures water transmission speed through the soil at a given time (Huggett, 2018). Clayey soil contains small clay particles (<2 m), tightly packed during sedimentation, creating numerous small pores and leading to high porosity.

The compacted particles limit the connectivity between voids, resulting in low permeability (Terzaghi & Peck, 1996). This reduced permeability hinders the drainage of water molecules infiltrating the ground, leading to water retention in the soil mass. Consequently, this water retention increases the weight of the soil mass, impacting the angle of safety and reducing the slope's shear strength, ultimately causing instability and landslides (Eric, 1996).

Active weathering processes in the research area are influenced by weather conditions, constituting the fourth factor contributing to the high percentage of clay minerals in the study location. Clay minerals are a product of chemical weathering prevalent in the wet tropical climate of the study area, characterized by high precipitation even during the dry season (Nelson, 2014). Chemical weathering involves the breakdown of substances through various chemical reactions, such as the formation of clay minerals like kaolinite from the hydrolysis of silicate mineral orthoclase, as demonstrated in the following equation (Birchmier, 2005). The increased production of clay minerals due to heightened weathering rates exacerbates the aforementioned issues.

$$4KAlSi_3O_8 + 4H^+ + 2H_2O \rightarrow 4K^+ + Al_4Si_4O_{10}(OH)_8 + 8SiO_2 \quad (1)$$

Based on the results of the mineralogy analysis, a predominant presence of the clay mineral kaolinite was observed in the specimens, which is regarded as less reactive compared to illite. Soil samples from location L1 exhibited seven distinct peaks of kaolinite as opposed to five peaks of illite. Similarly, soil samples from location L2 displayed five prominent peaks of kaolinite compared to four peaks of illite, while those from location L3 showcased five peaks of kaolinite instead of three peaks of illite. Despite the prevalence of kaolinite, the presence of illite in the soil composition could significantly enhance the adsorption of water molecules, thereby contributing to the aforementioned issues.

4. CONCLUSION

The shear strength values of the soil are significantly affected by the presence of clay minerals and the microfabric of the soil. The primary clay minerals identified in this study were kaolinite and illite. The shear strength values of the unaltered clayey soil samples ranged from 128.28 to 155.01 kPa, indicating a classification of strong soil. The specific arrangement of these minerals, forming assemblages that layer together, allowing for increased water absorption and discharge, notably impacts soil cohesion, which is a critical factor in determining the shear strength of slope materials. The prevalence of kaolinite and illite, particularly in a region characterized by high moisture levels, can significantly diminish soil cohesion, consequently lowering the shear strength of the slope materials as a whole. Clay minerals, due to their higher propensity for water absorption within their mineral structure compared to other minerals, play a crucial role in this process.

ACKNOWLEDGMENTS

This research was funded by the UMS Niche Fund Scheme (SDN) Research Grant SDN0037-2019 and Industrial Grant LPS2331. All experiments were conducted in the laboratories at the Faculty of Science and Natural Resources, University Malaysia Sabah.

REFERENCES

Andrei, A. B., Elena, G. U., & Hassan Y. A. (2015). X-ray diffraction: Instrumentation and applications. *Critical Reviews in Analytical Chemistry*, *45*(4), 289–299. https://doi.org/10.1080/10408347.2014.949616

ASTM International. (2012). *Standard test methods for laboratory compaction characteristics of soil using standard effort (12,400 ft-lbf/ft³ (600 kN-m/m³))* (ASTM D698-12). Advancing Standards Transforming Markets. https://store.astm.org/d0698-12r21.html

Azizi, H. A., Asupyani, H., Akbar, F., & Sulaksana, N. (2020). Landslide zoning with GIS analysis method: Case study cipelah and its surrounding area, Rancabali subdistrict, Bandung Regency, West Java. *IOP Conference Series: Earth and Environmental Science*, *412*(1), Article 012023. https://doi.org/10.1088/1755-1315/412/1/012023

Balasubramanian, A. (2017). *Characteristics of soil profile*. Centre for Advanced Studies in Earth Science, University of Mysore. https://www.researchgate.net/publication/314497793_CHARACTERISTICS_OF_SOIL_PROFILE

Birchmier, M. A. (2005). *Weathering effects on the mineralogy, chemistry and micromorphology of Pierre Shale* [Master's thesis, Iowa State University]. Iowa State University Digital Repository. https://dr.lib.iastate.edu/handle/20.500.12876/72863

Bowles, J. E. (2012). *Engineering properties of soils and their measurements* (4th ed.). McGraw Hill Education.

British Standards Institution. (1990). *Methods of test for soils for civil engineering purposes* (BS 1377-1:1990). BSI. https://knowledge.bsigroup.com/products/methods-of-test-for-soils-for-civil-engineering-purposes-general-requirements-and-sample-preparation-1

British Standards Institution. (2003). *Non-destructive testing—X-ray diffraction from polycrystalline and amorphous materials* (BS EN 13925-2:2003). BSI.

https://knowledge.bsigroup.com/products/non-destructive-testing-x-ray-diffraction-from-polycrystalline-and-amorphous-materials-procedures

British Standards Institution. (2016). *Microbeam analysis—scanning electron microscopy—guidelines for calibrating image magnification* (BS ISO 16700:2016-TC). BSI. https://knowledge.bsigroup.com/products/microbeam-analysis-scanning-electron-microscopy-guidelines-for-calibrating-image-magnification

Bullock, M. S., Nelson, S. D., & Kemper, W. D. (1988). Soil cohesion is affected by freezing, water content, time, and tillage. *Soil Science Society of America Journal*, *52*(3), 770–776. https://doi.org/10.2136/sssaj1988.03615995005200030031x

Eric, R. (1996). *Land husbandry components and strategy* (FAO Soils Bulletin 70). Food and Agriculture Organization of the United Nations. https://www.fao.org/4/t1765e/t1765e00.htm

Head, K. H. (1982). *Manual of soil laboratory testing* (2nd ed.). Pentec Press.

Huggett, J. M. (2018). Clay minerals. In *Encyclopedia of Geology* (2nd ed., pp. 358–365). Elsevier.

Jackson, N., & Dhir, R. K. (1996). Shear strength of soil. *Civil Engineering Materials*, *88*(c), 415–429.

Jacobson, G. (1970). *Gunung kinabalu area, sabah, malaysia* (Geological Survey of Malaysia Report 8). Geological Survey of Malaysia.

Jr. Joe, E., Tongkul, F., & Roslee, R. (2018). Engineering properties of debris flow material at Bundu Tuhan, Ranau, Sabah, Malaysia. *Pakistan Journal of Geology*, *2*(2), 22–26. https://doi.org/10.26480/pjg.02.2018.22.26

Juergen, H. S. (2011). *Physical properties of rock: A workbook* (8th ed.). Elsevier.

Malaysian Meteorological Department (Sabah). (2022). *Daily rainfall data for Mesilou Kundasang Agricultural Station and Tamu Darat Kota Belud Agricultural Station* (JMM/CSBH/0/600-06/5). Malaysian Meteorological Department (Sabah).

Mashiri, M. S., Vinod, J. S., Sheikh, M. N., & Tsang, H. H. (2015). Shear strength and dilatancy behaviour of sand-tyre chip mixtures. *Soils and Foundations*, *55*(3), 517–528. https://doi.org/10.1016/j.sandf.2015.04.004

Nelson, S. A. (2014). *Weathering & clay minerals* [Lecture notes]. Earth & Environmental Science 2110, Tulane University. https://www2.tulane.edu/~sanelson/eens211/weathering&clayminerals.htm

Prasad, N. B. N. (2017). *Landslides: Causes & mitigation*. Centre for Water Resources Development and Management. https://www.researchgate.net/profile/N-B-Prasad/publication/317328970_Landslides-Causes_Mitigation/links/593273670f7e9beee78d98e1/Landslides-Causes-Mitigation.pdf

Roslee, R. (2020). Effects of physical and mechanical properties of residual soil on sliding area at Bundu Tuhan, Sabah, Malaysia. *Geological Behavior*, *4*(1), 18–25. https://doi.org/10.26480/gbr.01.2020.18.25

Roslee, R., Tahir, S., & Laming, A. (2005). Engineering geological investigation on slope failure along Bundu Tuhan to Kundasang Road, Sabah, Malaysia. *Warta Geologi*, *31*(3), 75–104.

Roylance, D. (2001). *Stress–strain curves* [Lecture notes]. Department of Materials Science and Engineering, Massachusetts Institute of Technology. https://web.mit.edu/course/3/3.11/www/modules/ss.pdf

Sanudin, H. T., & Baba, M. (2007). *Pengenalan kepada stratigrafi*. Penerbit Universiti Malaysia Sabah.

Smith, R., Jahangir, M., & Rinker, W. (2006). Selection of design strengths for over consolidated clays and clay shales. In *Proceedings of the 40th Symposium on Engineering Geology and Geotechnical Engineering* (pp. 2–11). Utah State University. https://www.scribd.com/document/83484277/Design-Strengths-for-Over-Consolidated-Clays-and-Clay-Shales-Technical-Paper

Soehady Erfen, H. F. W., Musta, B., Kim, K.-W., & Kim, J. H. (2018). Moisture implication on landslide occurrences of lateritic soil slopes in Ranau, Sabah, Malaysia. *ASM Science Journal*, *11*(3), 178–186.

Suhaimi, D. N. A. A., & Selaman, O. S. (2013). A study on correlation between pore water pressure, rainfall and landslide occurrence. *Journal of Civil Engineering, Science and Technology*, *4*(2), 24–27. https://doi.org/10.33736/jcest.115.2013

Terezie, V., Jan, K., Jiri, C., Ladislav, B., & Ondrej, S. (2016). Evaluation of the parameters affecting the cohesion of fine-grained soil. *IOP Conference Series: Earth and Environmental Science*, *44*(2), Article 022019. https://doi.org/10.1088/1755-1315/44/2/022019

Terzaghi, K., & Peck, R. B. (1996). *Soil mechanics in engineering practice* (3rd ed.). John Wiley & Sons.

Valášková, M., & Martynková, G. S. (2012). Vermiculite: Structural properties and examples of the use. In M. Valášková & G. S. Martynková (Eds.), *Clay minerals in nature—Their characterization, modification and application* (pp. 209–238). IntechOpen. https://doi.org/10.5772/51237

Welton, J. E. (1984). *SEM Petrology Atlas* (AAPG Methods in Exploration Series No. 4). American Association of Petroleum Geologists. https://www.researchgate.net/profile/Elmar-Buchner-2/post/Is-there-any-recommendation-of-textbook-or-publication-to-study-mineral-identification-by-SEM-for-beginner/attachment/5ab222104cde266d5892d2d6/AS%3A606547348570114%401521623565994/download/sem-atlas.pdf

Yalcin, A. (2007). The effects of clay on landslides: A case study. *Applied Clay Science*, *38*(1–2), 77–85. https://doi.org/10.1016/j.clay.2007.01.007

Zhou, Z., Chen, S., Wang, Y., & Dai, Z. (2021). Crack evolution characteristics and cracking mechanism of red beds in central Sichuan during seepage and swelling. *Geofluids*, *2021*(1), Article 9981046. https://doi.org/10.1155/2021/9981046